ORIGINAL SCIENTIFIC PAPER

CROATICA CHEMICA ACTA

Croat. Chem. Acta **2019**, *92*(3), 357–367
Published online: July 29, 2019
DOI: 10.5562/cca3505

HKD 1926

A Computational Study of 2-(chloromethyl)oxirane Ring Opening by Bromide and Acetate Anions Considering Electrophilic Activation with Cations of Alkali Metals

Kseniia Yutilova,[1] Yuliia Bespal'ko,[2] Elena Shved[1,*]

[1] Educational and Scientific Institute of Chemistry, Vasyl' Stus Donetsk National University, 21 600-richchia Str., Vinnytsia 21021, Ukraine

[2] Department of Chemistry, University of Leuven, Celestijnenlaan 200 F box 2404, B-3001 Leuven (Heverlee) Belgium

* Corresponding author's e-mail address: o.shved@donnu.edu.ua

RECEIVED: February 19, 2019 * REVISED: July 1, 2019 * ACCEPTED: July 1, 2019

Abstract: Ring opening of 2-(chloromethyl)oxirane *via* the nucleophilic substitution with bromide and acetate anions was investigated using density functional theory (DFT) calculations. It was shown that the geometry of the transition states and the activation parameters of the reactions correspond to those of S_N2-like mechanism. The nature of localized transition states was analyzed using More O'Ferrall – Jencks plots. The quantum chemical simulations of the potential energy surface for the ring-opening reaction of oxirane by nucleophiles confirmed the theoretical assumptions about the favored path of interactions, which is a backside *α*-attack of nucleophile. The effect of alkali metal cation (Li^+, Na^+, K^+) on that path was estimated. It was found that the electrophilic activation with alkali metal cation is more pronounced in the reaction of 2-(chloromethyl)oxirane with dissociated ions, than with ionic pairs.

Keywords: 2-(chloromethyl)oxirane, alkali metal bromides, alkali metal acetates, nucleophilic substitution, mechanism, DFT calculations.

INTRODUCTION

RING-OPENING reaction of oxiranes by nucleophilic reagents (H-Nu) is a well-known chemical process widely used in organic synthesis.[1–3] The ring opening of the substituted oxiranes leads to a parallel formation of normal (*n*-P) and abnormal (*α*-P) products (Scheme 1), which are versatile intermediates in organic synthesis due to three reaction centers at contiguous carbon atoms.[4–8] Only normal product transformations allow obtaining the glycidyl esters, which are important compounds for polymer industry.[4–6,8–10] According to the Krasusky rule,[11] the formation of the *n*-P esters is favored[12–14] and is in good agreement with nucleophilic attack through S_N2 mechanism with some contribution of "borderline" S_N2-like mechanism.[15]

Scheme 1 exhibits the possible directions of attack by a nucleophilic reagent on both carbon atoms of the oxirane ring of 2-(chloromethyl)oxirane (epichlorohydrin,

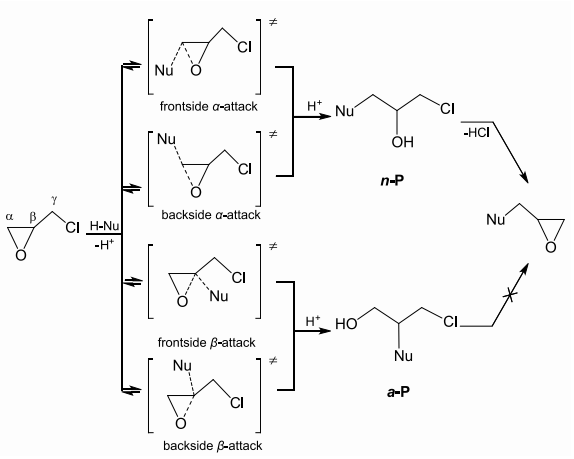

Scheme 1. Possible paths of nucleophilic attack (H-Nu) on 2-(chloromethyl)oxirane: formation of *n*-P and *α*-P products of ring-opening reaction and possible TS leading to these products

This work is licensed under a Creative Commons Attribution 4.0 International License.

ECH), leading to the formation of *n*-P and *a*-P products, as well as possible transition states (TS) leading to these products. Nucleophile may attack *α*- and *β*-carbons of the oxirane ring from two sides. In a frontside attack, the nucleophile attacks the electrophilic center on the same side as oxygen, and in a backside one, the nucleophile attacks carbon on the side of C–C bond. Any *α*-attack leads to formation of *n*-P product, while any *β*-attack results in *a*-P product. According to references,[11,16,17] the attack on *γ*-carbon does not proceed *via* classic S_N2 substitution, so it will not be further considered.

The regioselectivity of the oxirane ring-opening reactions depends on the structure of the oxiranes, acids and catalysts. Thus, acidolysis of phenyloxirane by acrylic and benzoic acids in the presence of tetrabutylphosphonium bromide results in normal product yield of 94 % and 66 %, respectively,[18] by acetic acid in the presence of anion exchange resin Purolite A500 – of 39–70 % depending on reaction temperature.[19] The yield of abnormal product may reach 20–50 % in some reaction series.[12,14,19] Establishing the aspects of the interaction between oxiranes and nucleophiles is the key to control of regioselectivity of the ring cleavage and to increase of yield of *n*-P.

Nucleophile particles in the "nucleophile-oxirane" reaction systems are usually attached to electrophiles; *e.g.*, reactants carrying both nucleophilic and electrophilic center, such as alcohols, phenols, carboxylic acids, quaternary ammonium or alkali metals halides and carboxylates, are used in the synthesis of glycidyl esters.[1,6,7,20] An investigation of special aspects of *n*-P ester formation includes consideration of the joint effect of electrophile and nucleophile.[21–23]

The ring opening of oxiranes by nucleophilic reagents (S_N2-like mechanism) may proceed without (A) and with (B) preliminary activation of oxirane ring by electrophile (without and with electrophilic activation) (Scheme 2), and the last one has an energetic benefit.[11,22] To consider the contribution of the electrophilic activation, it is important to model the ring-opening reaction by reagent containing both electrophilic and nucleophilic particles (E-Nu).

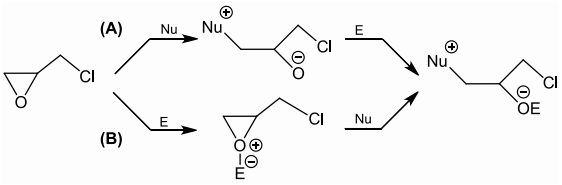

Scheme 2. Nucleophilic ring-opening of 2-(chloromethyl)-oxirane without (**A**) and with (**B**) electrophilic activation

An effective method for studying the mechanism of reaction (Scheme 1) and predicting its chemo-, regio-, and stereoselectivity is quantum chemical modelling of the potential energy surface (PES), which allows calculating the structure of possible TS, their kinetic and thermodynamic characteristics.[24] The predictive power of the computational approach was confirmed for the similar series "ECH – acetic acid – tertiary amine" with a high correlation of the calculated and experimental data,[25] which are comparable with calculated data on the oxirane ring opening in the series "glycidyl ether – carboxylic acid – amine".[26]

The aim of this work is to study the selectivity of the ring opening of an asymmetric oxirane in the system "ECH – E-Nu", where E is cation of an alkali metal and Nu is the bromide or acetate anion, by the method of quantum chemical modelling. The interaction between the E-Nu and ECH is a rate-determining step of the mechanism of catalytic oxirane ring opening, and its product is an intermediate which enters subsequent reactions with the formation of thermodynamically stable particles. Bromide anion represent the particle from the origin catalyst (tetraalkylammonium halide) and acetate anion is from the real catalyst, whose formation is expected during the reaction with acetic acid. Recent studies[27] showed that S_N2 reactions can proceed extremely well when halides react with alkali metal cation as counterion.

COMPUTATIONAL METHODS

ECH, nucleophiles and their ionic pairs (bromide anion; acetate anion; lithium, sodium, and potassium bromides and acetates) were chosen as modelling objects for Scheme 1. The choice is due to computational simplicity of this model[26,27] and its versatility for prediction of the experimental kinetic data. Thus, similar quantum chemical simulations were used in our previous works to predict the possibility of interaction, reactivity and mechanism in the reactions of anhydrous curing of epoxy resin ED-20[23,28] and ECH ring opening by benzoic acid.[30] Since the oxirane ring opening is carried out in an excess of ECH, it is difficult to model interactions in the system, where solvent directly participate in the reaction as a substrate. The study was carried out in the gas phase, as it was found that similar calculations for the reaction series "ECH – acetic acid – tertiary amine" showed a high adequacy to the experiment.[25]

Optimization of the geometry of TS, reactants, products of nucleophilic ring opening of ECH, bond orders calculations, and frequency analysis were performed by density functional theory (DFT) method with B3LYP exchange correlation functional and 6-31+G** basis set for the gas phase. Computations were executed in PC Firefly 8.2.0 program complex.[31] Building and visualizing the model objects structure was carried out in Chemcraft software.[32] Since ECH may exist in three conformer forms,[9,32] the most stable conformation (ap) of the

molecule was taken for computation. The geometry parameters of the initial ECH structure are given in SI, Table S1. Stationary structures are confirmed by ascertaining that all the harmonic frequencies are real. Structures of the transition state are obtained by only one imaginary harmonic frequency, and also by carrying out the intrinsic reaction coordinate (IRC) analysis along the reaction pathway.[15,25,27,33] Energy gradient threshold = 10^{-4} a.u., scale factor = 0.96 in all computations.[34,35] The harmonic frequencies were used to calculate activation energies E_a, enthalpies $\Delta H^{\ddagger}$, entropies $\Delta S^{\ddagger}$, and free energies $\Delta G^{\ddagger}$ at 298.15 K and 1 atm, using the standard formulas of statistic thermodynamics.[37] Zero point energies (ZPE) were taken into account. Reaction rate constants for the gas phase were estimated by the equation:

$$k(T) = k_B T/h \cdot \exp(-\Delta G^{\ddagger}/RT) \quad (1)$$

where k_B is Boltzmann constant, $1.381 \cdot 10^{-23}$ J K^{-1}; h is Planck constant, $6.626 \cdot 10^{-34}$ J s; R – universal gas constant, 8.314 J K^{-1} mol^{-1}.

RESULTS AND DISCUSSION

TS Geometry

As the main objective of this study is to establish the favored path of Scheme 1, modelling of the ring-opening reaction of ECH by bromide and acetate anions as nucleophiles was carried out. The structures of localized **TS 1-4** for bromide attack, **TS 5** for acetate attack, as well as orders of breaking and forming bonds, are represented in Figure 1. All of the other TS structures of acetate attack and bond orders are deposited in SI, Figure S2.

There are four possible attack ways: backside attack on α-carbon (**TS 1, 5**), frontside attack on α-carbon (**TS 2, 6**), backside one on β-carbon (**TS 3, 7**), and frontside one on β-carbon (**TS 4, 8**). Moreover, as acetate anion has more complex structure than bromide anion including two oxygen atoms, two possible configurations of one's attack should be considered: Z, where acetate anion lies on the same side of ring plane as chloromethyl group, and E, where acetate anion lies on the side of ring plane that is opposite to chloromethyl group (Figure 1, **TS 5(Z)** and **5(E)**).

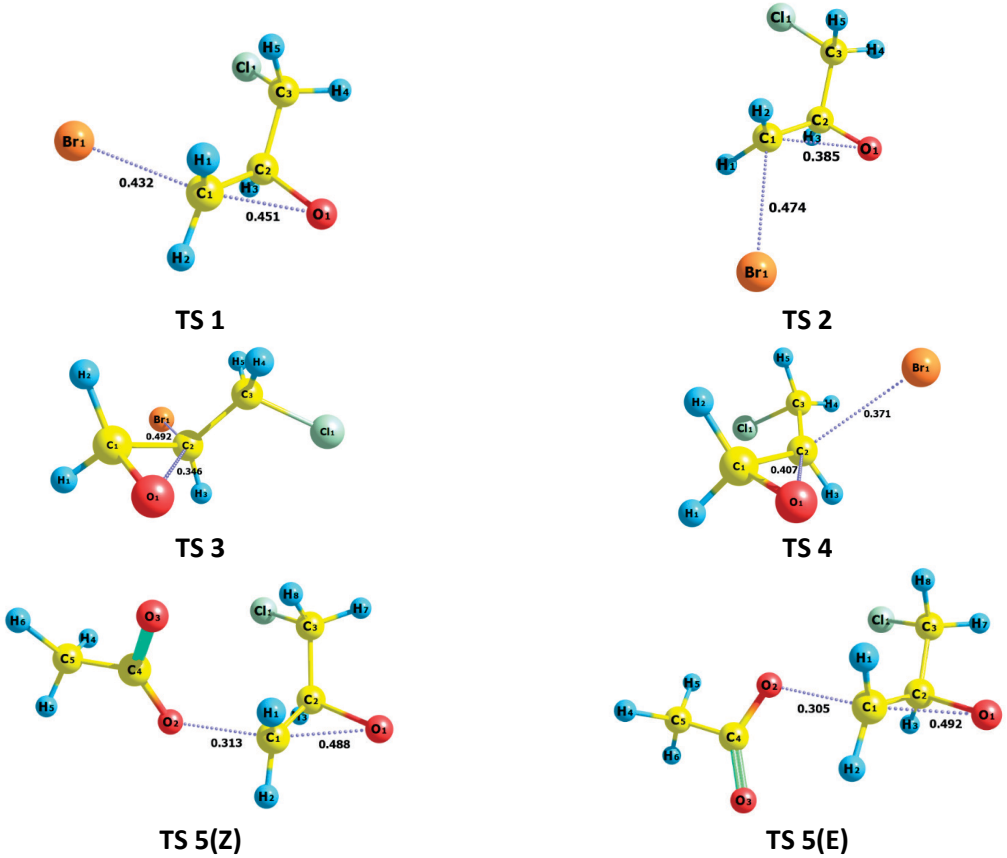

Figure 1. Geometry of the localized TS (B3LYP/6-31+G**, gas phase, 298.15 K) of the reaction of ECH with Br^-: **TS 1** – α-backside attack; **TS 2** – α-frontside attack; **TS 3** – β-backside attack; **TS 4** – β-frontside attack; with OAc^-: **TS 5(Z)** – α-backside attack on the side of chloromethyl group; **TS 5(E)** – α-backside attack opposite to chloromethyl group; the other TS structures of acetate attack are deposited in SI, Figure S2 (**TS 6** – α-frontside attack; **TS 7** – β-backside attack; **TS 8** – β-frontside attack)

As one can see from Figure 1, the angle between breaking and forming bonds for the backside attacks is close to 180 °, for the frontside ones to 90 °, and attacking nucleophile in **TS 1, 3, 5** and **7** lies in the oxirane ring plane, which is typical for S_N2 processes.[11] Deviation from the ring plane in case of the frontside attacks (**TS 2, 4, 6** and **8**) can be explained by considerable mutual repulsion of bromide anion and oxirane oxygen, as well as the steric effect of chloromethyl group in the *β*-frontside attack. The detailed geometry parameters of the obtained TS are listed in SI, Table S2.

Energy Profiles

While geometry of the localized TS gives primary concept of the behavior of the reaction of bromide and acetate anion with ECH, the activation parameters are important to know for reactivity estimation.

The energy profiles (Figure 2; SI, Figure S3) of Scheme 1 are obtained by IRC procedure.[28] Assuming the fact that the energy of TS of the ion-molecular reaction in the gas phase is lower than energy of the initial particles,[36,37] the "inner" activation barriers for this type of reaction are calculated as the difference between energies of TS and pre-reaction complex.[11,37] The structures of pre-reaction and post-reaction complexes in the ECH interaction with bromide anion are given in Figure 2. For all the other structures of initial and product complexes, see SI, Figure S1–S2.

In comparison with the frontside attack of bromide anion (reaction paths correspond to **TS 2** and **4**), pathways **1** and **3** have a small difference in energy between the transition and final states, and low activation energy. Therefore, **TS 1** and **3** are late, which is typical for endothermic processes.[26,36] As the product of the interaction between the anion and ECH is characterized by the high energy, it enters subsequent reactions on the way of ECH oxirane ring opening.

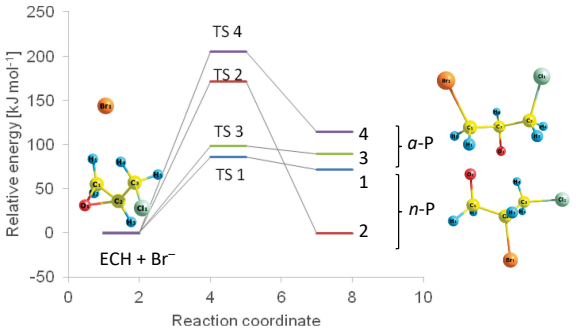

Figure 2. Energy profiles of the reaction of ECH with Br^- (B3LYP/6-31+G**, gas phase, 298.15 K): **TS 1** – *α*-backside attack; **TS 2** – *α*-frontside attack; **TS 3** – *β*-backside attack; **TS 4** – *β*-frontside attack; ECH + Br^- is the structure of the pre-reaction complex; *n*-P and *α*-P – structures of post-reaction complexes obtained from **TS 1-2** and **3-4**, respectively; energy profiles of ECH with OAc^- are deposited in SI, Figure S3.

For acetate anion (SI, Figure S3), pathways **5** and **6** do not have significant heat effect; reaction path **5** is even slightly exothermic, while pathways **7** and **8** are endothermic. For **TS 8**, energy profile is given for E configuration only, as the IRC calculation of **TS 8(Z)** has led to a cyclic product, which is not a product of the reaction under consideration.

Calculated values of the order of C–O bond cleavage and C–Nu bond formation in the TS (SI, Table S5) were used for building a More O'Ferrall – Jencks diagram,[39] a two-dimensional projection of the PES (Figure 3 and 4).

The ratio of breaking and forming bonds in TS may be assessed by one's location with respect to diagram diagonals. Attack of nucleophile on the reaction center (S_N) will generally proceed through one of three different pathways, *i.e.* associative, dissociative, and synchronous pathways.[40] An associative pathway for the nucleophilic substitution at the carbon atom is unlikely, since it should lead to the formation of a product with pentacoordinated carbon (the hypothetical structures of the product are given in the top left corners of Figure 3 and 4). A dissociative pathway results in the formation of a carbocation, the structure of which is represented in the bottom right corners of the diagrams. A third possibility is a synchronous S_N2-type mechanism, in which bond formation and cleavage occur in a single reaction step (diagonal from the bottom left to top right corners of Figure 3 and 4).[38,39] The points that lie to the left of this diagonal correspond to associative TS, and to the right - to dissociative ones.

The investigated reaction passes *via* a single transition state without an intermediate. For bromide ion attack, **TS 1** and **4** are a little to the right of the diagonal and hold on the middle position between pre-reaction complex and product, **TS 2** and **3** are more product-like, and for acetate anion attack, **TS 5-8** are dissociative and reactant-like.

The activation parameters of the ring-opening reaction of ECH by bromide and acetate anions are given in Table 1 (SI, Table S3). The most energetically profitable, according to Table 1, is the *α*-backside attack (**TS 1**), because the correspondent reaction proceeds with minimal energy in this position.

Effect of Cation

To estimate the effect of alkali metal cation, similar calculations were performed for lithium, sodium, and potassium bromides and acetates. Building of the initial structures was based on the backside attack on *α*-carbon,

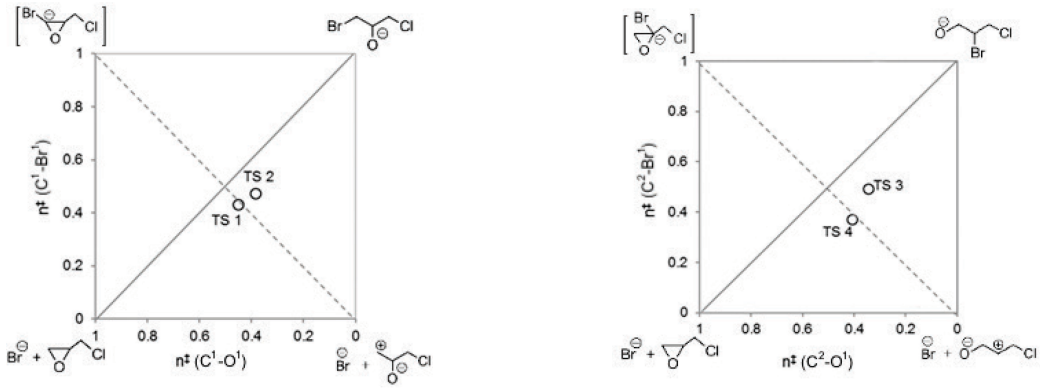

α-attack β-attack

Figure 3. More O'Ferrall – Jencks diagram of the reaction of ECH with Br^- (B3LYP/6-31+G**, gas phase, 298.15 K): **TS 1** – α-backside attack; **TS 2** – α-frontside attack; **TS** 3– β-backside attack; **TS 4** – β-frontside attack; $n^‡$ (C–O¹) and $n^‡$ (C–Br¹) – the orders of breaking and forming bonds, respectively (associative hypothetical structures of pentacoordinated carbon are in the top left corners, dissociative structures are in the bottom right ones).

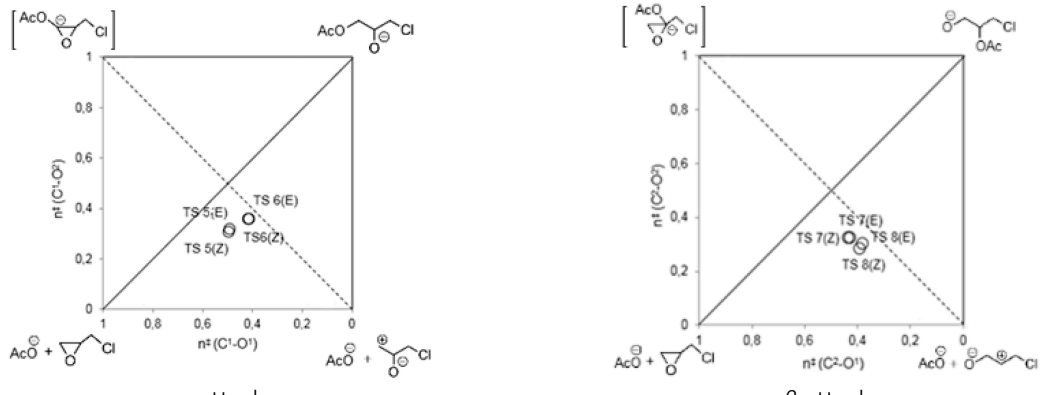

α-attack β-attack

Figure 4. More O'Ferrall – Jencks diagram of the reaction ECH with OAc^- B3LYP/6-31+G**, gas phase, 298.15 K): **TS 5** – α-backside attack; **TS 6** – α-frontside attack; **TS 7** – β-backside attack; **TS 8** – β-frontside attack; $n^‡$ (C–O¹) and $n^‡$ (C–O²) – the orders of breaking and forming bonds, respectively (associative hypothetical structures of pentacoordinated carbon are in the top left corners, dissociative structures are in the bottom right ones).

as the priority of this pathway of Scheme 1 was established. As provided above, bromide anion lies in the oxirane ring plane, while calculations showed that alkali metal cations are out of this plane. Depending on the location of cation, two configurations of bromides were obtained (Figure 5): Z, where cation lies on the same side of the ring plane as chloromethyl group, and E, where cation lies on the side of the ring plane that is opposite to chloromethyl group. As acetate anion itself forms two configurations with ECH, two structures of TS of alkali metal acetates with ECH are also located there: Z/Z, where both cation and anion lie at the same side of the ring plane as chloromethyl group, and E/E, where both cation and anion lie on the side of the ring plane that is opposite to chloromethyl group (Figure 5, **TS 14(Z/Z)** and **14(E/E)** for potassium acetate). All of the other TS structures of alkali metal acetate attack and bond orders are deposited in SI, Figure S5 (**TS 12** – LiOAc; **TS 13** – NaOAc). The interaction between the cation and Cl in chloromethyl group is minimal in ap-configuration of ECH. The investigation[15] of H_2O reaction with O-protonated ECH showed that no displacement of Cl and no interaction between proton and Cl of CH_2Cl was observed. So, in present work this possible interaction between alkali metal cation and Cl is considered to be absent. The structures of pre-reaction and post-reaction complexes in the ECH interaction with alkali metal bromides and acetates are given in SI, Figure S4–S5.

Placing alkali metal cation and acetate anion on the opposite sides of the ring was found to be unsuccessful and resulted in the same Z/Z and E/E configurations that were obtained before. The detailed geometry parameters of the TS are listed in SI, Table S4.

Table 1. Activation parameters, enthalpy change of reaction ($\Delta_r H$) and calculated rate constants ($k(T)$) for the ECH reaction with bromide (**TS 1-4**) and acetate (**TS 5-8**) anions; b – backside attack, f – frontside attack (B3LYP/6-31+G**, gas phase, 298.15 K)

TS	Direction	$\Delta H^{\ddagger}$ / kJ mol^{-1}	$\Delta S^{\ddagger}$ / J mol^{-1} K^{-1}	$\Delta G^{\ddagger}$ / kJ mol^{-1}	E_a / kJ mol^{-1}	$\Delta_r H$ / kJ mol^{-1}	$k(T)$ / s^{-1}
			α-attack				
1	b	79.39	–1.91	79.95	85.69	71.98	$6.09\cdot10^{-2}$
2	f	161.92	–12.91	165.77	170.96	46.99	$5.62\cdot10^{-17}$
			β-attack				
3	b	91.54	–14.29	95.81	98.50	88.90	$1.02\cdot10^{-4}$
4	f	195.82	–13.23	199.76	204.89	114.47	$6.22\cdot10^{-23}$
			α-attack				
5(Z)	b	69.63	–2.81	70.47	70.99	11.75	2.79
5(E)	b	50.63	–22.59	57.37	51.92	–9.29	$5.51\cdot10^{2}$
6(Z)	f	181.33	10.83	178.10	185.92	5.15	$3.88\cdot10^{-19}$
6(E)	f	155.84	–28.70	164.40	162.46	–5.94	$9.78\cdot10^{-17}$
			β-attack				
7(Z)	b	85.50	–26.19	93.31	90.33	44.31	$2.79\cdot10^{-4}$
7(E)	b	93.62	34.15	83.44	90.70	32.24	$1.50\cdot10^{-2}$
8(Z)	f	180.88	–15.46	185.49	188.64	–	$1.97\cdot10^{-20}$
8(E)	f	180.91	–3.67	182.01	188.01	45.38	$8.03\cdot10^{-20}$

Obtained values of the orders of C^1–O^1 bond cleavage and C^1–Nu bond formation in the TS (SI, Table S5) were used for building a More O'Ferrall – Jencks diagram (Figure 6). Compared to the **TS 1-8** with anions only, **TS 9-14** decline more from the S_N2 diagonal of the diagram and tend to form dissociative and more loose structures. Thus, TS of the reaction of ECH with alkali metal bromides and acetates are dissociative and reactant-like. TS of E configuration are earlier than Z configuration. Looseness of the TS decreases from lithium to potassium salts; this tendency is more noticeable in case of bromides.

Ion-pairing and Dissociation

An important purpose of modelling ECH interactions with alkali metal salts is establishing the favorable state of the E-Nu reagent in the reaction system (Figure 7): either in the form of dissociated ions (Br^-, OAc^-) or in the state of ionic pairs with metal cation (MBr, MOAc). Since dissociation is an endothermic process, expenditure of energy is required for bond cleavage. The energies of dissociation of ionic compounds, halides in particular, are very high in the gas phase. Thus, the energy of gas phase bond cleavage of Cs–Cl is 434 kJ mol^{-1}.[41] In the gas phase, a high activation barrier of the ring opening by dissociated ions involves two processes: the oxirane ring opening (low activation barrier) and dissociation (more than 400 kJ mol^{-1}). In the real system, while reaction is performed in epichlorohydrin, a solvent of medium polarity (ε = 22.6),[42] an alkali metal halide exists in the form of ion pairs and free ions formed in an exothermic process (Figure 8). Therefore, the total activation barrier of the process is lower for the state of free ions, since it has a small contribution of dissociation energy.

Activation energy of the ring opening of ECH decreases with increase of cation radius, *i.e.* from lithium to potassium salts, both in state of ionic pairs and dissociated ions. This may be expected, because the electrostatic influence of compact lithium cation is more significant than that of large potassium cation, which means stronger reduction of the nucleophilicity of anion by the smaller cations.[27] The reaction in the presence of free ions is highly exothermic, which gives it an advantage over the endothermic reaction with the ionic pairs.

The activation parameters of the interaction of ECH with alkali metal acetates and bromides are given in Table 2 (SI, Table S6). While the values of activation energy for different configurations are nearly the same for one cation, E configuration has insignificant energy gain. Alkali metal cation causes electrophilic activation in the investigated reaction series, which is conditioned by attraction of oxygen atom of ECH by cation and therefore by more effective cleavage of C–O bond. Considering the fact that cation radius increases from lithium to potassium, and taking into account the values of surface charge, it should be stated that lithium cation is stronger electrophile than potassium one. However, the less electrophilic properties

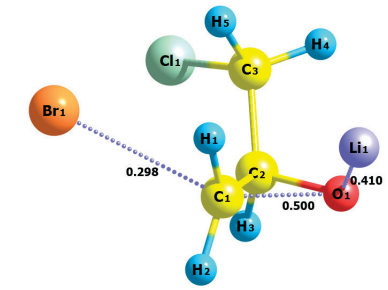

TS 9(Z)

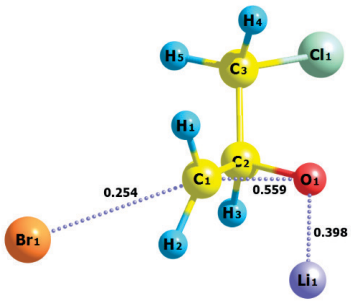

TS 9(E)

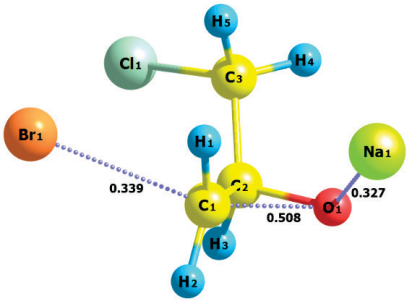

TS 10(Z)

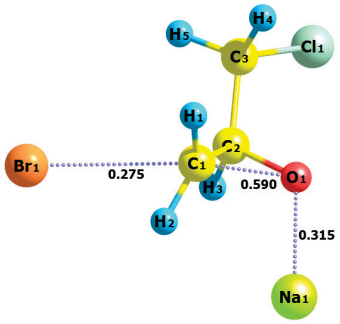

TS 10(E)

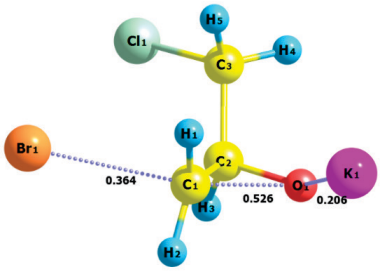

TS 11(Z)

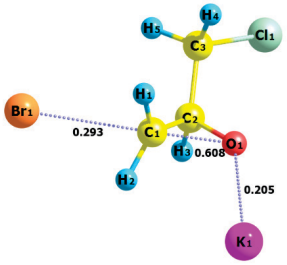

TS 11(E)

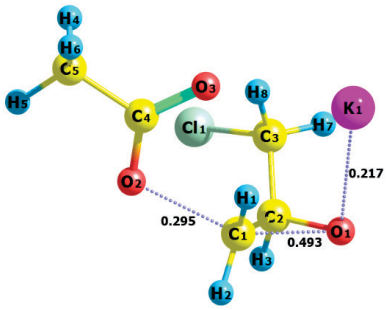

TS 14(Z/Z)

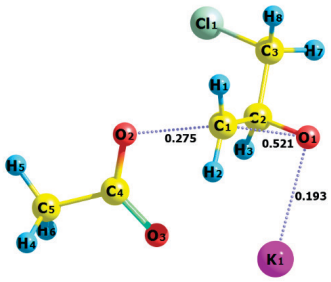

TS 14(E/E)

Figure 5. Geometry of localized TS of ECH reaction with MBr, backside α-attack (B3LYP/6-31+G**, gas phase, 298.15 K): **TS 9** – LiBr; **TS 10** – NaBr; **TS 11** – KBr; with KOAc: **TS 14(Z/Z) –** backside α-attack on the side of CH_2Cl, **TS 14(E/E) –** backside α-attack opposite to CH_2Cl. The other TS structures of alkali metal acetates attack and bond orders are deposited in SI, Figure S5 (**TS 12** – LiOAc; **TS 13** – NaOAc)

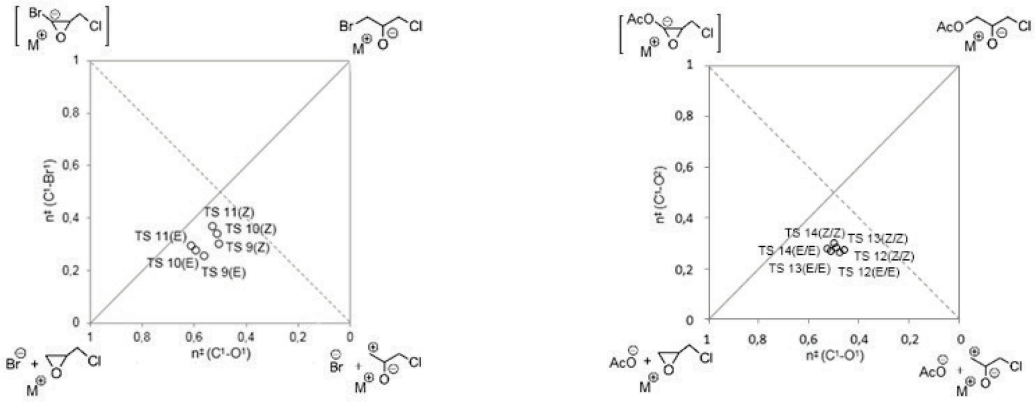

$M^+[ECH\cdots Br]^-$ $M^+[ECH\cdots OAc]^-$

Figure 6. More O'Ferrall – Jencks diagram for ECH complexes with alkali metal bromides (**TS 9** – LiBr; **TS 10** – NaBr; **TS 11** – KBr) and acetates (**TS 12** – LiOAc; **TS 13** – NaOAc; **TS 14** – KOAc), backside α-attack (B3LYP/6-31+G**, gas phase, 298.15 K); $n^{\ddagger}$ (C^1–O^1) – the order of breaking bond in both complexes with bromides and acetates; $n^{\ddagger}$ (C^1–Br^1) and $n^{\ddagger}$ (C^1–O^2) – the orders of forming bonds in the complexes with bromides and acetates, respectively (associative hypothetical structures of pentacoordinated carbon are in the top left corners, dissociative structures are in the bottom right ones).

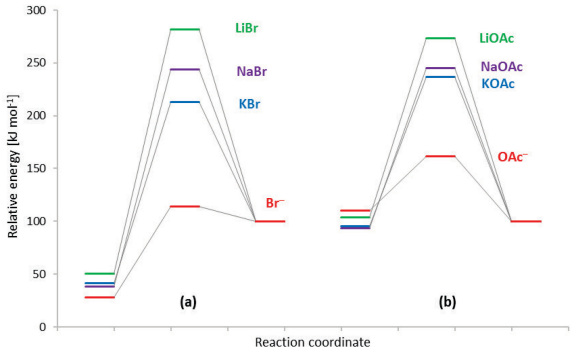

Figure 7. Energy profiles of the attack on ECH with bromides **(a)**: Br^- – **TS 1**, LiBr – **TS 9(E)**, NaBr – **TS 10(E)**, KBr – **TS 11(E)**; and acetates **(b)**: OAc^- – **TS 5(E)**, LiOAc – **TS 12(E/E)**, NaOAc – **TS 13(E/E)**, KOAc – **TS 14(E/E)**; B3LYP/6-31+G**, gas phase, 298.15 K.

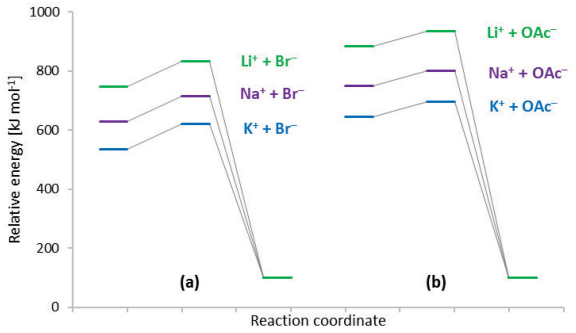

Figure 8. Energy profiles of the attack on ECH with **(a)** bromides (**TS 1**) and **(b)** acetates (**TS 5(E)**) of alkali metals in dissociated state; B3LYP/6-31+G**, gas phase, 298.15 K.

and the bigger cation radius of potassium represent the favorable conditions for coordination of nucleophile and oxirane into unique structure (TS) in the investigated series. These conditions promote the increase of nucleophilic attack rate on carbon atom of oxirane. Then, the interaction of ECH with potassium salts has the lowest activation energy and, respectively, the highest reaction rate.

These conclusions confirm the behavior of ionic catalysts of ECH ring opening that were obtained experimentally for acetates and given in the fundamental work.[43] For the reaction of ECH with acetic acid in the presence of acetates of alkali metals and quaternary ammonium, the catalytic reaction rate constants rise with increase of cation radius (Table 3). Therefore, the obtained simulation data are sufficient to predict the catalytic activity of alkali metal halides and acetates in the reaction of the oxirane ring opening of ECH.

CONCLUSION

Oxirane ring-opening interaction with bromides and acetates of alkali metals belongs to the S_N2 reactions. The backside attack by bromide anion and backside E-attack by acetate anion on α-carbon have the lowest activation energies (85.69 and 51.92 kJ mol^{-1}, correspondingly). Energy barriers for Z and E configurations of acetate anion demonstrate close values within one attack pathway. The transition states of reaction of ECH with alkali metal bromides and acetates have dissociative nature according to obtained More O'Ferrall – Jencks plots. Potassium salts exhibit the highest efficiency of nucleophilic epoxide ring opening in the explored reaction series. Electrophilic activation of the ring opening of 2-(chloromethyl)oxyrane

Table 2. Activation parameters, enthalpy change of reaction ($\Delta_r H$) and calculated rate constants ($k(T)$) for the reaction of ECH with alkali metal (M) bromides (**TS 9-11**) and acetates (**TS 12-14**), backside α-attack (B3LYP/6-31+G**, gas phase, 298.15 K)

TS	M^+	$\Delta H^‡$ / kJ mol^{-1}	$\Delta S^‡$ / J mol^{-1} K^{-1}	$\Delta G^‡$ / kJ mol^{-1}	E_a / kJ mol^{-1}	$\Delta_r H$ / kJ mol^{-1}	$k(T)$ / s^{-1}
9(Z)	Li^+	236.52	–0.10	236.55	244.12	52.82	$2.24\cdot10^{-29}$
9(E)	Li^+	225.83	15.25	221.28	231.05	49.33	$1.06\cdot10^{-26}$
10(Z)	Na^+	214.26	3.05	213.35	221.16	104.91	$2.59\cdot10^{-25}$
10(E)	Na^+	199.55	–1.13	199.88	205.92	62.03	$5.92\cdot10^{-23}$
11(Z)	K^+	183.11	5.06	181.60	189.07	93.56	$9.45\cdot10^{-20}$
11(E)	K^+	166.15	7.69	163.86	171.69	58.72	$1.21\cdot10^{-16}$
12(Z/Z)	Li^+	188.45	–34.62	198.77	193.14	1.52	$9.27\cdot10^{-23}$
12(E/E)	Li^+	164.57	–44.49	177.84	169.46	–3.86	$4.32\cdot10^{-19}$
13(Z/Z)	Na^+	169.29	–32.70	179.04	173.62	13.60	$2.66\cdot10^{-19}$
13(E/E)	Na^+	148.89	–24.50	156.19	151.24	6.12	$2.68\cdot10^{-15}$
14(Z/Z)	K^+	148.10	–30.81	157.29	152.36	9.87	$1.72\cdot10^{-15}$
14(E/E)	K^+	127.81	–25.42	135.39	132.43	5.06	$1.18\cdot10^{-11}$

Table 3. The effect of cation nature and size of catalyst on the rate of ethylene oxide reaction with acetic acid, 90 °C [43]

Salt	$10^4 k_{kat}$ / M^{-2} s^{-1}	Cation radius / Å	Anion radius / Å
LiOAc	1.35	0.78	1.56
NaOAc	1.80	0.98	
KOAc	2.17	1.33	
Me_4NOAc	4.80	3.47	
Et_4OAc	5.30	4.00	
Bu_4OAc	6.52	4.94	

by the metal cation in the series from lithium to potassium increases significantly in the state of dissociated ions compared to ionic pairs. Since the actual process is carried out in a solvent, where the energy costs for dissociation are low, alkali metal salts take part in the reaction predominantly in the state of free ions (attack energy barrier 50–90 kJ mol^{-1}) compared to ionic pairs (over 150 kJ mol^{-1}). Obtained computational data form the framework for prediction of the ring-opening reaction of 2-(chloromethyl)oxirane in the presence of alkali metal salts.

Acknowledgment. The study was carried out within the Fundamental Research Programme funded by the Ministry of Education and Science of Ukraine (Project No. 0116U002519).

Supplementary Information. Supporting information to the paper is attached to the electronic version of the article at: http://doi.org/10.5562/cca3505.

PDF files with attached documents are best viewed with Adobe Acrobat Reader which is free and can be downloaded from Adobe's web site.

REFERENCES

[1] J. Herzberger, K. Niederer, H. Pohlit, J. Seiwert, M. Worm, F. R. Wurm, H. Frey, *Chem. Rev.* **2016**, *116*, 2170–2243. https://doi.org/10.1021/acs.chemrev.5b00441

[2] M.-P. Pham, Theoretical studies of mechanisms of epoxy curing systems, The University of Utah, Salt Lake City, **2011**, pp. 9-10.

[3] A. Bukowska, K. A. Guskov, M. G. Makarov, E. Rokaszewski, V. F. Shvets, *J. Chem. Technol. Biotechnol.* **1995**, *63*, 374–378. https://doi.org/10.1002/jctb.280630411

[4] M. Mascioni, N. N. Ghosh, J. M. Sands, G. R. Palmese, *J. Appl. Polym. Sci.* **2013**, *130*, 479–486. https://doi.org/10.1002/app.39184

[5] J. Chen, X. Nie, Z. Liu, Z. Mi, Y. Zhou, *ACS Sustain. Chem. Eng.* **2015**, *3*, 1164–1171. https://doi.org/10.1021/acssuschemeng.5b00095

[6] D. C. McLeod, N. V. Tsarevsky, *Macromolecules* **2016**, *49*, 1135–1142. https://doi.org/10.1021/acs.macromol.5b02437

[7] G. Ahn, S. Kweon, C. Yang, J. E. Hwang, K. Kim, B. S. Kim, *J. Polym. Sci. Part A Polym. Chem.* **2017**, *55*, 4013–4019. https://doi.org/10.1002/pola.28865
[8] M. M. Movsumzade, M. I. Shatirova, U. S. Dzhafarova, N. K. Niyazova, *Russ. J. Gen. Chem.* **2018**, *88*, 389–392. https://doi.org/10.1134/S1070363218030027
[9] G. S. Singh, K. Mollet, M. D'Hooghe, N. De Kimpe, *Chem. Rev.* **2013**, *113*, 1441–1498. https://doi.org/10.1021/cr3003455
[10] Z. S. Bassampour, S. M. Budy, D. Y. Son, *J. Appl. Polym. Sci.* **2017**, *134*, 44620. https://doi.org/10.1002/app.44620
[11] L. I. Kasian, A. O. Kasian, S. I. Okovityi, I. N. Tarabara, *Alitciklicheskie epoksidnye soedineniia. Reaktcionnaia sposobnost* [*Alicyclic epoxy compounds. Reactivity*], Izdatelstvo Dnepropetrovskogo universiteta, Dnipropetrovsk, **2003**, pp. 17–51.
[12] R. Selvin, H.-L. Hsu, T.-M. Her, *React. Kinet. Catal. Lett.* **2009**, *96*, 75–82. https://doi.org/10.1007/s11144-009-5329-7
[13] M. Zhang, W. C. Huang, Y. Qin, Z. X. Huang, *Adv. Mater. Res.* **2010**, *150–151*, 1254–1257. https://doi.org/10.4028/www.scientific.net/AMR.150-151.1254
[14] M. A. Sinel'nikova, E. N. Shved, *Russ. J. Org. Chem.* **2014**, *50*, 332–336. https://doi.org/10.1134/S107042801403004X
[15] E. S. Shields, G. N. Merrill, *J. Phys. Org. Chem.* **2007**, *20*, 1058–1071. https://doi.org/10.1002/poc.1255
[16] D. M. Burness, *J. Org. Chem.* **1964**, *29*, 1862–1864. https://doi.org/10.1021/jo01030a047
[17] E. E. Ergozhin, K. I. Imanbekov, *Kvantovo-himicheskie aspekty sinteza amino- i piridinsoderzhashhih ionitov na osnove jepoksidnyh soedinenij* [*Quantum chemistry aspects of amino- and pyridine- containing ionites synthesis based on epoxy compounds*], Print-S, Almaty, **2007**, pp. 64–68.
[18] J. W. Kim, D. W. Cho, G. Park, S. H. Kim, C. S. Ra, *Bull. Korean Chem. Soc.* **2013**, *34*, 2286–2290. https://doi.org/10.5012/bkcs.2013.34.8.2286
[19] E. I. Muresan, T. Malutan, *Chem. Ind. Chem. Eng. Quaterly* **2009**, *15*, 169–174. https://doi.org/10.2298/CICEQ0903169M
[20] A. Bukowska, W. Bukowski, *Org. Process Res. Dev.* **2002**, *6*, 234–237. https://doi.org/10.1021/op010112q
[21] S. Bakhtin, Y. Bespal'ko, E. Shved, *React. Kinet. Mech. Catal.* **2016**, *119*, 139–148. https://doi.org/10.1007/s11144-016-1051-4
[22] S. Bakhtin, E. Shved, Y. Bespal'ko, *J. Phys. Org. Chem.* **2017**, *30*, e3717. https://doi.org/10.1002/poc.3717
[23] Y. N. Bespalko, M. A. Sinel'nikova, E. N. Shved, *Vopr. Khimii i Khimicheskoi Tekhnologii (Issues of Chemistry and Chemical Technology)* **2019**, *1*, 11–17. http://dx.doi.org/10.32434/0321-4095-2019-122-1-11-17
[24] M. Jaraíz, L. Enríquez, R. Pinacho, J. E. Rubio, A. Lesarri, J. L. López-Pérez, *J. Org. Chem.* **2017**, *82*, 3760–3766. https://doi.org/10.1021/acs.joc.7b00220
[25] Yu. N. Bespalko, E. N. Shved, *React. Kinet. Mech. Catal.* **2019**, *109*, 903–919. https://doi.org/10.1007/s11144-018-01524-2
[26] U. Q. Ly, M. P. Pham, M. J. Marks, T. N. Truong, *J. Comput. Chem.* **2017**, *38*, 1093–1102. https://doi.org/10.1002/jcc.24779
[27] J. Y. Kim, D. W. Kim, C. E. Song, D. Y. Chi, S. Lee, *J. Phys. Org. Chem.* **2013**, *26*, 9–14. https://doi.org/10.1002/poc.3010
[28] J. Li, X. Z. Yu, K. Zhang, *Adv. Mater. Res.* **2011**, *221*, 180–183. https://doi.org/10.4028/www.scientific.net/AMR.221.180
[29] E. N. Shved, M. A. Sinel'nikova, Y. N. Bespal'ko, N. M. Oleinik, K. V. Agapiy, L. A. Kolodina, *Voprosy Khimii i Khimicheskoi Tekhnologii (Issues of Chemistry and Chemical Technology)* **2012**, *1*, 80.
[30] E. A. Bakhalova, Y. M. Bespalko, E. M. Shved, *Bull. Dnipropetr. Univ. Ser. Chem.* **2017**, *25*, 65–72. https://doi.org/10.15421/081710
[31] A. A. Granovsky, "*Firefly* (formerly *PC GAMESS*)." Moscow, **2013**. http://classic.chem.msu.su/gran/gamess/
[32] G. A. Andrienko, "*Chemcraft*." Moscow, **2018**. https://www.chemcraftprog.com/
[33] F. Wang, P. L. Polavarapu, *J. Phys. Chem.* **2000**, *104*, 6189–6196. https://doi.org/10.1021/jp000757c
[34] A. V. Nemukhin, B. L. Grigorenko, A. A. Granovsky, *Moscow Univ. Chem. Bull.* **2004**, *45*, 75–102.
[35] A. P. Scott, L. Radom, *J. Phys. Chem.* **1996**, *100*, 16502–16513. https://doi.org/10.1021/jp960976r
[36] Y. Bouteiller, J. C. Gillet, G. Gregoire, J. P. Schermann, *J. Phys. Chem. A* **2008**, *112*, 11656–11660. https://doi.org/10.1021/jp805854q
[37] E. V. Anslyn, D. A. Dougherty, *Modern physical organic chemistry*, University Science, Sausalito, **2006**, pp. 68–71, 366.
[38] I. Novakovskaia, *Opredelenie termodinamicheskikh i kineticheskikh kharakteristik elementarnykh reaktcii na osnove kvantovokhimicheskikh raschetov* [*Determination of termodynamic and kinetic characteristics of elementary reactions based on quantum chemistry computations*], Moscow State University, Moscow, **2010**, pp. 14–27, 52–53.

[39] E. V. Jennings, K. Nikitin, Y. Ortin, D. G. Gilheany, *J. Am. Chem. Soc.* **2014**, *136*, 16217–16226. https://doi.org/10.1021/ja507433g

[40] S.-L. Chen, *Quantum Chemical Modeling of Binuclear Zinc Enzymes*, Royal Institute of Technology, Stockholm, **2008**, pp. 26–27.

[41] N. M. Emanuel, D. G. Knorre, *Kurs khimicheskoi kinetiki* [*The course of chemical kinetics*], Vysshaia shkola, Moscow, **1984**, pp. 26–28.

[42] D. R. Lide (ed.), *CRC Handbook of Chemistry and Physics*, CRC Press, Boca Raton, **2004**, p. 6-157.

[43] A. K. Guskov, S. Yui, M. G. Makarov, V. F. Shvets, *Kinet. Catal.* **1994**, *35*, 873.